Supplemental Information: Phonons and Elasticity of Cementite through the Curie Temperature

L. Mauger,[1] J. E. Herriman,[1] O. Hellman,[1] S. J. Tracy,[1] M. S. Lucas,[2] J. A. Muñoz,[1] Yuming Xiao,[3] J. Li,[4] and B. Fultz[1]

[1] *California Institute of Technology, W. M. Keck Laboratory 138-78, Pasadena, CA 91125, USA*
[2] *Air Force Research Laboratory, Wright-Patterson AFB, OH 45433, USA*
[3] *HPCAT, Geophysical Laboratory, Carnegie Institute of Washington, Argonne, IL 60439, USA*
[4] *Department of Earth and Environmental Sciences, University of Michigan, Ann Arbor, MI, USA*

(Dated: September 5, 2016)

I. STRUCTURE OF CEMENTITE

Cementite has an orthorhombic structure with the *Pnma* space group, containing 12 iron atoms and 4 carbon atoms per unit cell. The Fe atoms occupy two distinct sites on the lattice, with eight Fe_{II} atoms occupying the general site (8d), and four Fe_{I} occupying the special site (4c). The carbon atoms also occupy a 4c site, with prismatically coordinated positions between the Fe atoms.

The lattice parameters of our Fe_3C sample were extracted from x-ray diffraction measurement conducted using a laboratory Cu Kα source, shown in Fig. 1. The refined XRD pattern included MgO peaks which were remnants of the MgO capsule used in the high-pressure, high-temperature synthesis[1].

The experimental and computed equilibrium lattice parameters from this study are compared with other literature values in Table I. The lattice parameters calculated by DFT are in good agreement with the exception of the b lattice parameter, which appears slightly lower than previously reported results. The lattice positions of each of the unique crystal sites are shown in Table II. The calculated and experimentally-determined lattice sites are also in close agreement with previous results.

Table I. Unit cell parameters of cementite from various experimental and computational studies.

Source	**a** (Å)	**b** (Å)	**c** (Å)	Method
this study	5.0429	6.7028	4.4816	PAW/PBE
Jiang[3]	5.04	6.72	4.48	PAW/PBE
Dick[4]	5.035	6.716	4.480	PAW/PBE
Nikolussi[5]	5.036	6.724	4.480	PAW/PBE
Haeglund[6]	5.089	6.743	4.523	LMTO
this study	5.084(1)	6.751(1)	4.518(1)	Exp. (300K)
Wood[7]	5.081	6.753	4.515	Exp. (300K)
Gao[8]	5.0814	6.751	4.516	Exp. (300K)
Wood[7]	5.082	6.733	4.512	Exp. (4K)

Each Fe atom has a C atom first-nearest neighbor coordination shell, and an Fe atom second-nearest neighbor shell. The first-nearest neighbor carbon shells have similar interatomic distances for both Fe_{I} and Fe_{II} sites. The second-nearest neighbor coordination shells of Fe_{II} sites had a smaller average bond length than the second-nearest neighbor coordination shells of the Fe_{I} sites. The Fe_{II} atoms have the shortest Fe-Fe interatomic distances, aligned along the b-axis. Our computed local structure agrees with that reported by Fasiska et al.[9]

Table II. Unit cell parameters of the unique crystallographic sites in cementite from experiment and computation in fractional coordinates.

Method	Fe_{I} x,y,z	Fe_{II} x,y,z	C x,y,z
PAW/PBE	0.036,0.250,0.837	0.176,0.068,0.332	0.877,0.250,0.438
PAW/PBE[3]	0.036,0.250,0.837	0.176,0.068,0.332	0.876,0.250,0.438
300K Exp.	0.035,0.250,0.838	0.185,0.059,0.334	0.898,0.250,0.447
300K Exp.[7]	0.035,0.250,0.838	0.185,0.059,0.334	0.898,0.250,0.447

II. SELF-CONSISTENT CALCULATION OF ELASTIC CONSTANTS FROM FORCE CONSTANTS

We have calculated elastic constants by a novel self-consistent method. This method solves for the elastic constants of a system by direct comparison to calculated phonon frequencies at low $\boldsymbol{q}$ generated from DFT force constant calculations. The availability of this alternative is important because only the on-diagonal elements of a system's elastic matrix (in Voigt notation, elements C_{ij}) are well-defined by the Christoffel equations.

The self-consistent method relies on calculations of the dynamical matrix $\boldsymbol{D}(\boldsymbol{q})$, built from interatomic force constants, and an analogous $\boldsymbol{A}(\boldsymbol{q})$, built from elastic constants.[10] The eigenvalues of $\boldsymbol{A}(\boldsymbol{q})$ define the acoustic branches at a given $\boldsymbol{q}$ point, and therefore can be mapped to a subset of the spectrum of $\boldsymbol{D}(\boldsymbol{q})$, which defines both acoustic and optical phonon branches of a non-monoatomic crystal lattice.

To calculate the elastic constants C_{ij} self-consistently, the first calculation of $\boldsymbol{A}(\boldsymbol{q})$ is seeded with values of C_{ij} calculated from the Born-Huang relations.[10] The $\boldsymbol{A}(\boldsymbol{q})$ is then iteratively refined from the reference spectrum provided by $\boldsymbol{D}(\boldsymbol{q})$ and the eigenvectors of the previous iteration for $\boldsymbol{A}(\boldsymbol{q})$ until the spectrum of $\boldsymbol{A}(\boldsymbol{q})$ converges to the values provided by $\boldsymbol{D}(\boldsymbol{q})$.

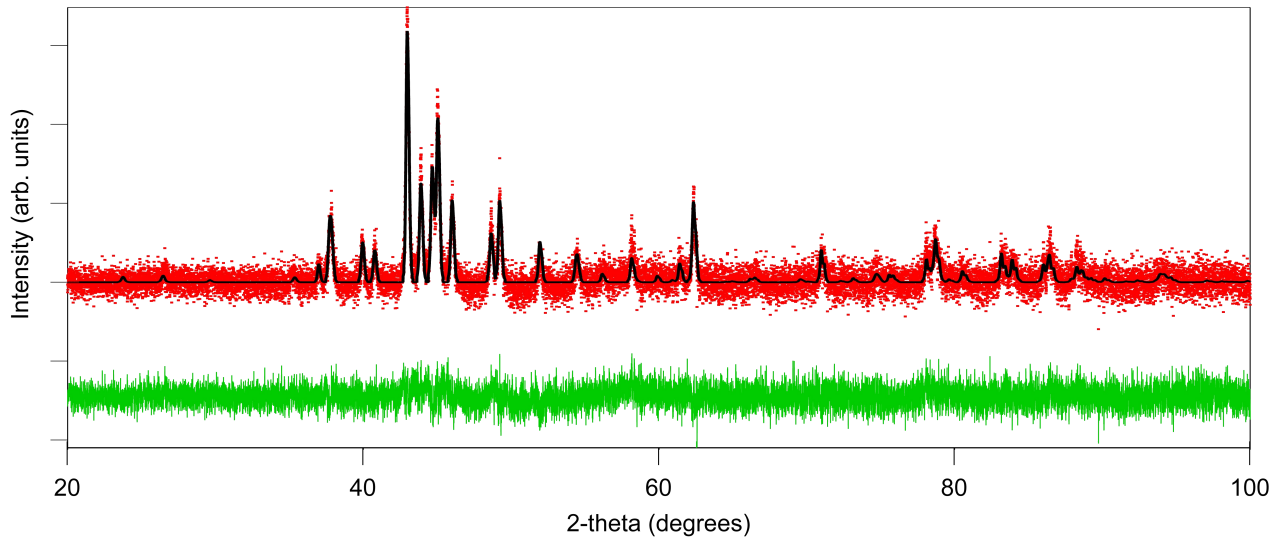

Figure 1. (Color online) Powder x-ray diffraction pattern of the Fe_3C collected on a Cu Kα laboratory source (red), analyzed using Rietveld refinement methods (black)[2], with the difference offset below (green). The refinement included MgO impurity peaks (remnants of the synthesis capsule) which were used as an internal calibrant.

A. Background for the Self-Consistent Method

The relationship between elastic constants and force constants is well defined for long wavelengths by the Born-Huang relations.[10] These relationships can also be understood by relating the dynamical matrix $\boldsymbol{D}(\boldsymbol{q})$, built from force constants, to an analogous matrix $\boldsymbol{A}(\boldsymbol{q})$, built from elastic constants.

The release of an inhomogeneous stress on a crystal triggers elastic displacements described by Fourier components

$$\boldsymbol{u}(\boldsymbol{x}) = \boldsymbol{u}(\boldsymbol{q}) \exp\left(i\left[\boldsymbol{q}\cdot\boldsymbol{x} - \omega(\boldsymbol{q})t\right]\right) \tag{1}$$

such that

$$\rho\omega^2(\boldsymbol{q})\boldsymbol{u}(\boldsymbol{q}) = \boldsymbol{A}(\boldsymbol{q})\boldsymbol{u}(\boldsymbol{q}) \tag{2}$$

where ρ is the density of the crystal and ω is a frequency corresponding to one of the three acoustic branches at point $\boldsymbol{q}$. The expression for elements of $\boldsymbol{A}(\boldsymbol{q})$ is

$$A_{\alpha\beta}(\boldsymbol{q}) = \sum_{\gamma\lambda} C_{\alpha\gamma,\beta\lambda} q_\gamma q_\lambda \tag{3}$$

Equation 2 takes on a form similar to

$$\omega^2(\boldsymbol{q})\boldsymbol{U}(\boldsymbol{q}) = \boldsymbol{D}(\boldsymbol{q})\boldsymbol{U}(\boldsymbol{q}) \tag{4}$$

which results from the following trial solution to the equations of motion for a system of N atoms

$$u_\alpha\begin{pmatrix} l \\ k \end{pmatrix} = \frac{1}{\sqrt{m_k}} U_\alpha\left(k|\boldsymbol{q}\right) \exp\left(i\left[\boldsymbol{q}\cdot\boldsymbol{x}(l) - \omega(\boldsymbol{q})t\right]\right) \tag{5}$$

For these equations, the $3N \times 3N$ matrix $\boldsymbol{D}(\boldsymbol{q})$ is defined by

$$\boldsymbol{D}(\boldsymbol{q}) = \begin{pmatrix} \boldsymbol{D}\begin{pmatrix} \boldsymbol{q} \\ 11 \end{pmatrix} & \ldots & \boldsymbol{D}\begin{pmatrix} \boldsymbol{q} \\ 1n \end{pmatrix} \\ \ldots & \ldots & \ldots \\ \boldsymbol{D}\begin{pmatrix} \boldsymbol{q} \\ n1 \end{pmatrix} & \ldots & \boldsymbol{D}\begin{pmatrix} \boldsymbol{q} \\ nn \end{pmatrix} \end{pmatrix} \tag{6}$$

$$\boldsymbol{D}\begin{pmatrix} \boldsymbol{q} \\ kk' \end{pmatrix} = \begin{pmatrix} D_{xx}\begin{pmatrix} \boldsymbol{q} \\ kk' \end{pmatrix} & D_{xy}\begin{pmatrix} \boldsymbol{q} \\ kk' \end{pmatrix} & D_{xz}\begin{pmatrix} \boldsymbol{q} \\ kk' \end{pmatrix} \\ D_{yx}\begin{pmatrix} \boldsymbol{q} \\ kk' \end{pmatrix} & D_{yy}\begin{pmatrix} \boldsymbol{q} \\ kk' \end{pmatrix} & D_{yz}\begin{pmatrix} \boldsymbol{q} \\ kk' \end{pmatrix} \\ D_{zx}\begin{pmatrix} \boldsymbol{q} \\ kk' \end{pmatrix} & D_{zy}\begin{pmatrix} \boldsymbol{q} \\ kk' \end{pmatrix} & D_{zz}\begin{pmatrix} \boldsymbol{q} \\ kk' \end{pmatrix} \end{pmatrix} \tag{7}$$

$$D_{\alpha\beta}\begin{pmatrix} \boldsymbol{q} \\ kk' \end{pmatrix} = \frac{1}{\sqrt{m_k m_{k'}}} \sum_{l'=1}^{p} \phi_{\alpha\beta}\begin{pmatrix} l, l' \\ k, k' \end{pmatrix} \times \exp\left(i\boldsymbol{q}\cdot\left[\boldsymbol{x}(l') - \boldsymbol{x}(l)\right]\right) \tag{8}$$

B. Description of the method

Our self-consistent method relies on solution of the elastic constants from a set of matrices $\boldsymbol{A}(\boldsymbol{q})$ defined for a set of points $\boldsymbol{q}$, sampled uniformly in a region of the Brillouin zone near the Γ point. To determine $\boldsymbol{A}(\boldsymbol{q})$ accurately, an estimate of the elastic constants is made using the Born-Huang relations, allowing for an initial construction of $\boldsymbol{A}(\boldsymbol{q})$. The matrices $\{\boldsymbol{A}(\boldsymbol{q})\}$ are then progressively refined using the the spectra of the corresponding set $\boldsymbol{D}(\boldsymbol{q})$ in conjunction with the eigenvectors of $\boldsymbol{A}(\boldsymbol{q})$.

The steps are:

1. Estimate the elastic constants $C_{\alpha\gamma,\beta\lambda}$ using the Born-Huang relations and the force constants obtained from phonon calculations.

2. For a set of points $\{\boldsymbol{q}\}$, construct a set of matrices $\{\boldsymbol{A}(\boldsymbol{q})\}$ using estimates for the elastic constants.

3. Calculate the eigenvalues and eigenvectors of each matrix in $\{\boldsymbol{A}(\boldsymbol{q})\}$.

4. Using the force constants obtained from phonon calculations, construct the matrix $\boldsymbol{D}(\boldsymbol{q})$ for each of the points in $\{\boldsymbol{q}\}$, used in step 2, and calculate its eigenvalues.

5. For each value of $\boldsymbol{q}$, calculate the eigenvalues of the corresponding matrices $\boldsymbol{A}(\boldsymbol{q})$ and $\boldsymbol{D}(\boldsymbol{q})$. Select the subset of eigenvalues of $\boldsymbol{D}(\boldsymbol{q})$ that correspond to the eigenvalues of $\boldsymbol{A}(\boldsymbol{q})$.

6. For each value of $\boldsymbol{q}$, calculate a refined version of the matrix $\boldsymbol{A}(\boldsymbol{q})$ by using a modified factorization of $\boldsymbol{A}(\boldsymbol{q})$ such that

$$\boldsymbol{A}(\boldsymbol{q})_{refined} = \tilde{\boldsymbol{u}}\rho\Omega\tilde{\boldsymbol{u}}^{-1} \tag{9}$$

   where $\tilde{\boldsymbol{u}}$ is a matrix containing the eigenvectors, $\{\boldsymbol{u}\}$, of $\boldsymbol{A}(\boldsymbol{q})$, ρ is the density, and Ω is a diagonal matrix containing the eigenvalues of $\boldsymbol{D}(\boldsymbol{q})$ that correspond to those of $\boldsymbol{A}(\boldsymbol{q})$.

7. Calculate the elastic constants $\{C_{\alpha\gamma,\beta\lambda}|1 \leq \alpha,\beta,\gamma,\lambda \leq 3\}$ from the refined set of matrices $\{\boldsymbol{A}(\boldsymbol{q})\}$.

8. Repeat steps 2 through 6 until the elastic constants have converged.

III. SYNCHROTRON EXPERIMENTS

High-temperature nuclear resonant inelastic x-ray scattering (NRIXS) measurements were performed in two independent sets to verify the anomalous elevated temperature behavior of ferromagnetic Fe_3C. Additionally a separate ambient temperature powder measurement (labeled 297K in manuscript Fig. 2) was collected for comparison at room temperature. The phonon partial DOS measurements from manuscript Fig. 2 are separated into the two sets of sequential measurements in Fig.2 and Fig. 3 below.

Nuclear forwarding scattering (NFS) measurements were collected at several temperatures immediately prior to NRIXS scans, as shown in Fig. 4. These spectra exhibit a clear magnetic beat pattern at 300K, similar to previous NFS measurements of Fe_3C[8,11,12]. The NFS spectra no longer exhibit a magnetic beating pattern at 463K, suggesting a loss of net magnetization at and above this temperature.

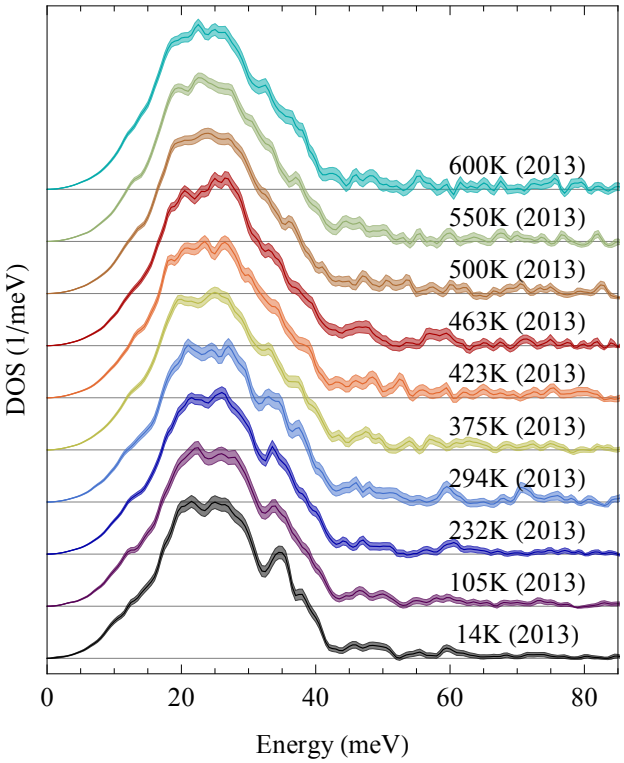

Figure 2. (Color online) NRIXS measurements of Fe_3C at several temperatures. The spectra below 295K were collected in a Be dome cryostat. The spectra at and above 295K were collected in series using the NRIXS furnace.

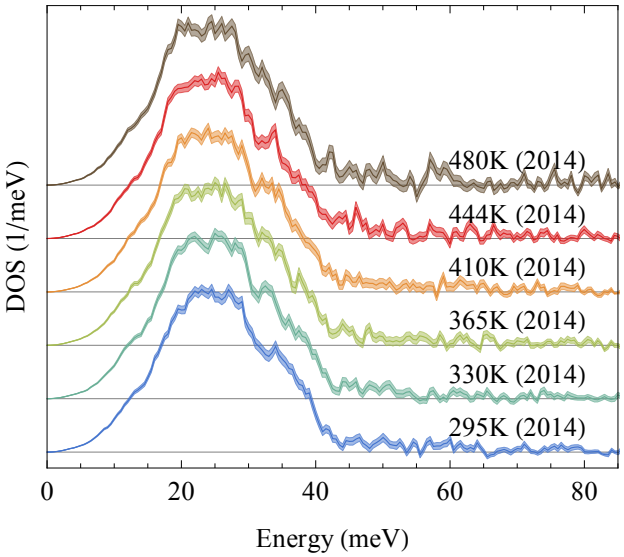

Figure 3. (Color online) NRIXS measurements of Fe_3C at several temperatures. These spectra were collected in series using the NRIXS furnace.

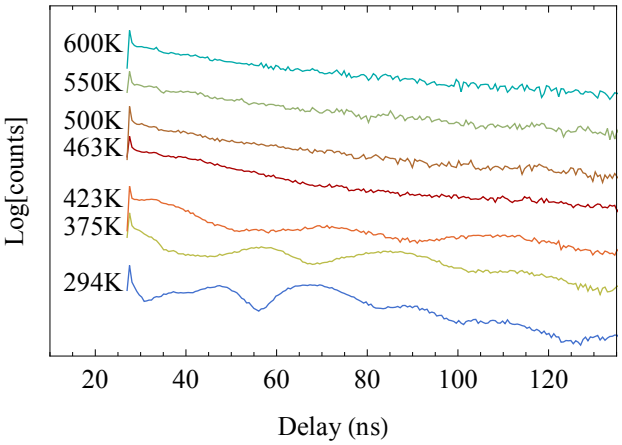

Figure 4. (Color online) Nuclear forward scattering measurements of Fe_3C at several temperatures. The spectra are displayed using a log scale, and offset for clarity.

Table III. The total vibrational entropy calculated from NRIXS Fe pDOS and DFT C pDOS.

Temperature (K)	Total S_{vib} k_B/atom
14	0.003 ± 0.000
105	0.744 ± 0.001
232	2.205 ± 0.002
294	2.786 ± 0.004
295	2.783 ± 0.004
297	2.794 ± 0.004
330	3.088 ± 0.005
365	3.351 ± 0.007
375	3.429 ± 0.008
410	3.658 ± 0.009
423	3.745 ± 0.010
444	3.880 ± 0.011
463	4.007 ± 0.012
480	4.113 ± 0.013
500	4.238 ± 0.014
550	4.520 ± 0.016
600	4.792 ± 0.019

IV. TOTAL VIBRATIONAL ENTROPY

Total vibrational entropy of cementite can be calculated by summing $S^{Fe}_{vib}(T)$ from NRIXS with $S^{C}_{vib}(T)$ from calculations. The values provided in Table III include a harmonic $S^{C}_{vib}(T)$ contribution calculated from the 0K DFT C pDOS. The errors provided encapsulate both the calculated quasiharmonic and anharmonic C phonon shifts, which contribute approximately 0.01 k_B per atom at T_C and oppose each other in sign.

The vibrational entropy values in Table III differ from the quasi-harmonic DFT study of Dick, et al.[4] by around $0.17 k_B$/atom at T_C. This disparity is mostly due to the fact that reported DFT phonon energies of Fe_3C are about 5.5% higher than experimentally observed phonon energies, which were used in this largely experimental assessment of the entropy.

V. ELECTRONIC DOS

The electron density of states (eDOS) calculated for cementite at 0K is shown in Fig 5, with the electronic contributions resolved into their orbital characters. The eDOS projected onto the carbon site lacks *d*-electron character, as expected. The carbon site electron DOS shows a large, deeply bound concentration of *p*-electrons below the Fermi surface, similar to findings from Khmelevskyi, et. al.[3,13] This is contrary to the simple suggestion that the thermal expansion anomaly in Fe_3C might be explained by how carbon atoms donate their conduction electrons, increasing the Fe valence to levels comparable to the FeNi invar composition. The Fe_{II} majority site eDOS has a larger concentration of electrons at the Fermi level than the minority Fe_I site. The Fe_{II} majority site has a large *d*-electron feature at energies just below the Fermi level. The high temperature eDOS at 400K shows no major change in features, aside from a general thermal smoothing. At 400K, the Fe_{II} site has a larger increase in electrons at the Fermi level than the Fe_I site. The calculated eDOS at the two Fe sites both undergo 7% increases in their *d*-electron occupations at the Fermi level, but the Fe_{II} site also shows a 4% increase in *p*-electron levels. While the calculated magnetic moments on both Fe sites remain nearly constant in high temperature CVFT calculations, their differing electronic character is suggestive of different behavior with temperature.

[1] D. Walker, R. Dasgupta, J. Li, and A. Buono, Contributions to Mineralogy and Petrology **166**, 935 (2013).
[2] A. C. Larson and R. B. V. Dreele, "General Structure Analysis System," (1990).
[3] C. Jiang, S. G. Srinivasan, A. Caro, and S. A. Maloy, Journal of Applied Physics **103**, 043502 (2008).
[4] A. Dick, F. Körmann, T. Hickel, and J. Neugebauer, Physical Review B **84**, 125101 (2011).
[5] M. Nikolussi, S. L. Shang, T. Gressmann, A. Leineweber, E. J. Mittemeijer, Y. Wang, and Z. K. Liu, Scripta Materialia **59**, 814 (2008).
[6] J. Häglund, G. Grimvall, and T. Jarlborg, Physical Review B **44**, 2914 (1991).
[7] I. G. Wood, L. Vocadlo, K. S. Knight, D. P. Dobson, W. G. Marshall, G. D. Price, and J. Brodholt, Journal of Applied Crystallography **37**, 82 (2004).

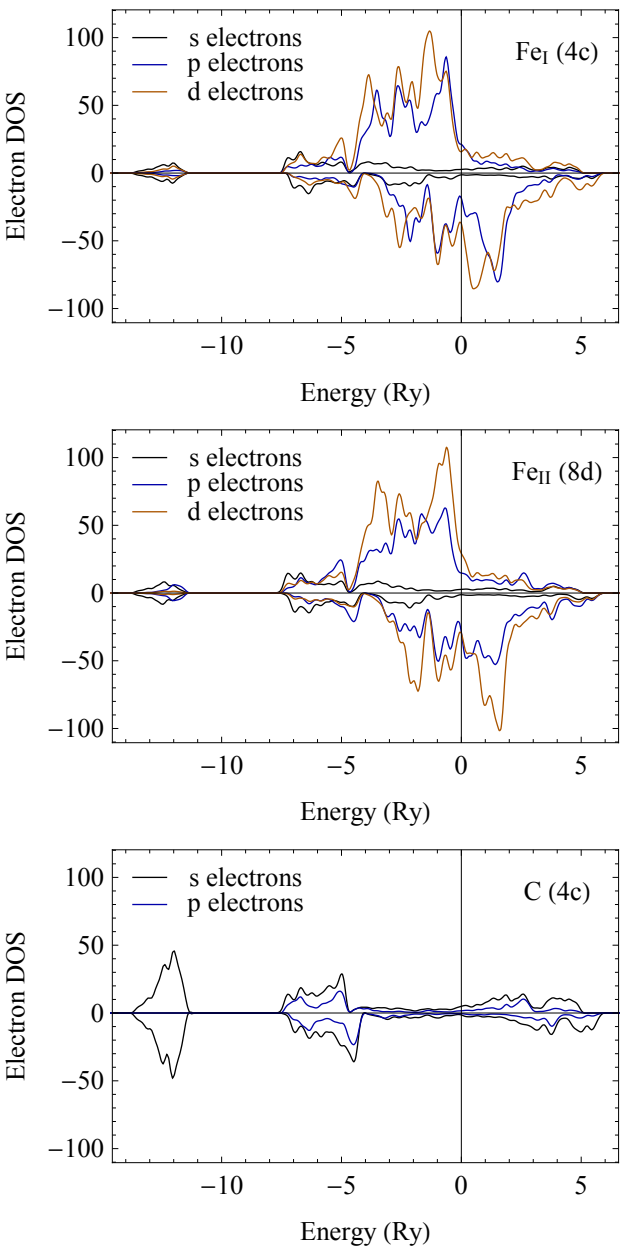

Figure 5. (Color online) The calculated electronic DOS, resolved into orbital contributions at the three distinct lattice sites.

[8] L. Gao, B. Chen, J. Wang, E. E. Alp, J. Zhao, M. Lerche, W. Sturhahn, H. P. Scott, F. Huang, Y. Ding, S. V. Sinogeikin, C. C. Lundstrom, J. D. Bass, and J. Li, Geophysical Research Letters **35**, L17306 (2008).

[9] E. J. Fasiska and G. A. Jeffrey, Acta Crystallographica **19**, 463 (1965).

[10] G. Venkataraman, L. A. Feldkamp, and V. C. Sahni, *Dynamics of perfect crystals* (MIT Press, 1975).

[11] L. Gao, B. Chen, M. Lerche, E. E. Alp, W. Sturhahn, J. Zhao, H. Yava, and J. Li, Journal of Synchrotron Radiation **16**, 714 (2009).

[12] L. Gao, B. Chen, J. Zhao, E. E. Alp, W. Sturhahn, and J. Li, Earth and Planetary Science Letters **309**, 213 (2011).

[13] S. Khmelevskyi, A. V. Ruban, and P. Mohn, Journal of Physics: Condensed Matter **17**, 7345 (2005).